Assessment of CO_2 dynamics in subsurface atmospheres using the wavelet approach: from cavity-atmosphere exchange to anthropogenic impacts in Rull cave (Vall d´Ebo, Spain)

Concepcion Pla [1,2*]; Juan Jose Galiana-Merino [3]; Soledad Cuezva [4]; Angel Fernandez-Cortes [4,5]; Juan Carlos Cañaveras [1,2]; David Benavente [1,2].

(1) Departamento Ciencias de la Tierra y del Medio Ambiente. Universidad de Alicante. Campus San Vicente del Raspeig s/n, 03690 San Vicente del Raspeig (Alicante).

(2) Laboratorio de Petrología Aplicada. Unidad Asociada CSIC-Universidad de Alicante. Campus San Vicente del Raspeig s/n, 03690 San Vicente del Raspeig (Alicante).

(3) Departamento Física, Ingeniería de Sistemas y Teoría de la Señal. Universidad de Alicante. Campus San Vicente del Raspeig s/n, 03690 San Vicente del Raspeig (Alicante).

(4) Museo Nacional de Ciencias Naturales (CSIC). José Gutiérrez Abascal, 2. 28006 Madrid.

(5) Department of Earth Sciences, Royal Holloway, University of London, Egham, Surrey TW20 0EX, UK.

*Corresponding author: c.pla@ua.es

Dpto. Ciencias de la Tierra y del Medio Ambiente. Universidad de Alicante. Campus San Vicente del Raspeig s/n, 03690 San Vicente del Raspeig (Alicante). Telephone: +34965903400 ext. 2095.

Abstract

Subsurface environments are non-negligible contributors to the net carbon balance because they act as natural sinks of CO_2 and are responsible for the efflux to the Earth´s atmosphere during their ventilation states. In this way, the characterization of the CO_2 dynamics in these underground environments is essential to determine the gas exchange between both atmospheres. A complete microclimatic analysis and trace gas (CO_2 and ^{222}Rn) monitoring of Rull cave (southeast Spain) were conducted to characterize the natural dynamics and anthropogenic influence on the cavity. The analysis was accomplished by implementing wavelet analysis and resemblance techniques. This study enhances wavelet analysis as an efficient tool to analyse microclimatic time series, as it allows for the detection of the main periodicities of signals located in the time domain and the prevailing relationships between them. The analysis indicates that the low-frequency components of the signals were close to the identified annual natural cycles. For a one-year cycle, the ventilation of the cavity causes the CO_2 concentration to decrease from 3,569 to 932 ppm in nearly one month, highlighting the existence of an output efflux from the cavity. On the contrary, the high-frequency components are linked to human perturbations caused by visitors in the cavity.

Key words: Wavelet analysis, seasonal and transient patterns, microclimatic monitoring, underground atmosphere, cave management.

1. Introduction

CO_2 exchange between terrestrial ecosystems and the atmosphere becomes crucial to understanding the feedbacks between climate change, net carbon balance and the land surface (Frisia et al. 2011). Plenty of CO_2 is contained in the soil surface and subterranean environments, turning these environments into non-negligible contributors in the global CO_2 balance, which should not be underestimated (Bourges et al. 2014; Cuezva et al. 2011; Kell 2012; Serrano-Ortiz et al. 2010, Pu et al. 2014).

The migration of CO_2 contained in the enriched vadose zone, primarily of an edaphic origin, is responsible for the accumulation of this gas in the underground cavities. In this regard, underground environments from the vadose zone can, in some cases, exceed the volumetric CO_2 fraction of 5% (Benavente et al. 2010; Sanchez-Cañete et al. 2013; Peyraube et al. 2013) that represents a CO_2 concentration more than 100 times larger than the one registered in the external atmosphere.

Subsurface environments are subjected to different mechanisms that derive from recharge, isolation and storage processes, characterized by significant seasonal, and even daily, variations (Fernandez-Cortes et al. 2011a; Garcia-Anton et al. 2014). According to previous studies, caves experience ventilation states responsible for the release of stored CO_2 to the Earth's atmosphere. The average net CO_2 outgassing from

underground cavities varies depending on the study site. For instance, some estimations of outgassing CO_2 fluxes established values of 120 mol day^{-1} on average for the Hollow Ride cave (Kowalczk and Froelich 2010), 2.34 to 11.71 kg day^{-1} for Grotta di Ernesto (Frisia et al. 2011) and up to 7600 mol day^{-1} (approximately 335 kg day^{-1}) for the Ojo Guareña karst system (Fernandez-Cortes et al. 2015).

Underground cavities are defined by the stability of their indoor climatic conditions. Occasionally, these environments have become tourist attractions where large numbers of people can be counted every year (Docampo et al. 2011). As a result, visitors generate an additional anthropogenic input of CO_2 (Faimon et al. 2006) or airborne microorganisms (Docampo et al. 2011; Fernandez-Cortes et al. 2011b).

To characterize and understand the dynamics of these natural systems, it is essential to study their microclimatic data series (Bourges et al. 2014; Frisia et al. 2011; Mattey et al. 2010). For instance, studying the variations in the ^{222}Rn concentrations is of great interest in subterranean environments (Valladares et al. 2014), as they are good indicators of the connection with the atmosphere not influenced by anthropogenic impacts. Because ^{222}Rn is chemically inactive, the balance of its sources and sinks is much simpler than those of other trace gases (Pitari et al. 2014). In cave climate studies, ^{222}Rn (abundant in caves) has often been used as an excellent tracer for air circulation (Gregorič et al. 2014).

To obtain helpful conclusions from the recorded data, a full analysis is required that allows for identifying the interaction between several factors and for detecting long trend behaviours affecting the data. The parameters monitored inside the caves allow for assessing the impact of visitors to the underground atmosphere. For cave managers, who oversee serious efforts to accomplish the protection and conservation of these environments, the study of cave dynamics has been a useful tool.

Currently, analyses of the non-stationary signals are accomplished by signal processing techniques, which have not usually been applied to cave microclimate data due to the absence of a specific methodology. The study and comparison of microclimatic signals should be focused on detecting the relationships between them. Therefore, the analysis would allow for establishing new conclusions about the microclimatic dynamics and trace gases in cavities and other underground environments.

The identification of the prevailing relationships between CO_2 concentration and microclimates in the underground atmosphere, which entirely contribute to the gas exchange with the outdoor atmosphere, can be improved when a proper analysis is applied. To develop an effective data analysis, some tools, which have been applied to other research fields, can also be applied to microclimatic data series as a novel application. For instance, segmentation methods have been successfully applied to tunnel boring (Denis and Cremoux 2002) and in detecting the mechanical behaviour of different geological formations (Frantziskonis and Denis 2003); spectral techniques have been used in analyses of precipitation (Li et al. 2014); wavelet analysis has been employed, for instance, for studies of environmental variables such as soil variations (Milne and Lark 2009), seismic wave characterization (Galiana-Merino et al. 2011), the

identification of karst spring systems (Chinarro et al. 2012), long-term aerosol concentration changes (Pal and Devara 2012) and atmospheric boundary layer dynamics and the impact on trace gas variability (Pal et al. 2014, 2015). Wavelet analysis is applied to reveal information on the periodicities present in data series. It enables filtering of raw signals of monitored factors by removing the non-useful parts of the recorded measures. In contrast to Fourier analysis, which only probes frequency characteristics of the signal, wavelets are localized in both time and frequency domains simultaneously.

The aim of this paper is to characterize the behaviour of CO_2 in the cavity to better understand the seasonal and transient behaviour of gas exchange between outdoor and indoor atmospheres. For this purpose, wavelet and resemblance techniques are performed and applied to the recorded signals in Rull cave, which represents a complete example of a touristic cavity in a typical Mediterranean climate. The analysis will allow differentiating between the stable natural trends in microclimatic signals and the human induced perturbations caused by visitors in the cavity.

2. Materials and methods

2.1. Study site

Rull cave (38^0 48' 40"N; 0^0 10' 38"W) is located in the north-eastern area of Alicante province, on the Spanish Mediterranean coast (30 km far from the coast line). The cave is located in massive Miocene conglomerates, which present textural and petrophysical complexity (De Carvalho et al. 2013) and were deposited on Cretaceous limestones. The overlying soil has a thickness of about 1 m with predominant silty texture and no differentiated horizons. The cavity mainly consists of an almost rounded shape, which comprises a total area of 1,535m^2. Cave ceiling reaches a maximum height of 20 metres in the central chamber, and the relative thickness of the overlying host rock varies from 9.3 to 22.3 metres. The study area is characterised by a thermo-Mediterranean sub-humid climate (Rivas-Martinez 1984). Inside the cave, calcite speleothems such as stalactites, columns, curtains or crusts are common, and fallen blocks of different sizes are present due to old ceiling collapses (Pla et al. 2015). Currently, the cavity has a single entrance shut by a door (approximately 3m^2) located at the top part of the cave, at the highest level. Rull cave is a tourist cavity, which has been equipped to attract visitors and spotlights and concrete corridors have been installed to allow people moving around easily when visiting the cave. Visitors annual average value is 13,265 (20,129 people in the studied period). Maximum number of visits occurred in summer and Easter Holidays. For the whole studied period, average value of visitors was 41 people per day. The cave remains annually closed for a 30 days period between January and February. Visits are organised in groups formed by an average value of 6 people but depending on the characteristics of the visit (scholars,

groups of people, individual families, etc.) more than 100 people can enter into the cave simultaneously. The visits get into the cave every 20 minutes and the guides perform visits twice an hour approximately.

2.2. Monitoring system

A microenvironmental monitoring system was installed to record microclimatic data on cave air from May 2013 to September 2014. The principal monitoring system consisted of one complete station with an 8-channel, 16-bit datalogger (COMBILOG TF 1020, Theodor Fiedrich & Co., Germany), RAM memory (512 Mb) and RS232 communication system. Although it is connected to the electrical power supply, the system is also provided with two security batteries that assure 14 hours of autonomy. The station scanned the connected probes every 10 seconds and recorded 15 minutes averages. Air temperature and relative humidity were measured by a HygroClip S3 sensor (Pt100 1/10 DIN temperature sensor and a Rotronic humidity sensor). Measurement ranges were from -40 to 100^0C and 0-100% with accuracies of ± 0.1^0C and ±0.8% respectively. Atmospheric pressure was measured with a silicon capacitive sensor Vaisala BAROCAP-PTB 100 (Finland) with a measure range and accuracy of 800-1,100 ± 0.3hPa. A non-dispersive infrared analyser ITR 498, ADOS (Germany), 0-10,000 ppm measurement range and 0.3% accuracy with a suction pump was used to measure CO_2 concentrations.

Radon concentrations were determined with a Radim 5WP Radon monitor (SSM&SISIE-Prague). The device was designed to support high humidity conditions. The measurement range is 80 to 50,000 Bq m^{-3} with a measurement interval of 30 minutes. In addition 3 extra control points were located inside the cave and were equipped with an autonomous datalogger, which stored 15-min average values of the air temperature and relative humidity (HOBO U23 Pro v2, Onset, Bourne, MA, USA).

Outside the cave, a weather station with an independent data logger (HOBO U30, Onset, Bourne, MA, USA) recorded air temperature, relative humidity, barometric air pressure, rainfall and wind (speed and direction) values every 15 minutes.

2.3. Time-frequency analysis

The different components of the microclimatic signals are obtained and evaluated. At first, data series are studied separately. Afterwards, wavelet analysis is performed for each data series, and relationships between pairs of time series are highlighted by cross analysis.

Wavelet transform is a successful technique to capture the characteristics and to detect localized phenomena in non-stationary time series (Rajaee 2011, Pal et al. 2012). By implementing wavelet analysis, a signal can be analysed at different time-frequency resolutions through scaled and translated versions (wavelets) of a basis function called a mother wavelet. In this work, continuous wavelet transform (CWT) and discrete wavelet transform (DWT), which are briefly described in the following paragraphs, are

implemented. For a deeper theoretical knowledge of the subject, some interesting references can be consulted (e.g., Daubechies 1992; Kaiser 1994; Strang and Nguyen 1996; Wickerhauser 1994).

Relative to the studied signals, i.e., microclimatic data series, the term period (inverse of frequency) is more suitable to be used. Thus, in the subsequent explanations and analyses, the frequency and time-frequency domains are converted to period and time-period domains, respectively. Therefore, the periodicities of the prevailing factors can be highlighted in a more intuitive way.

The principal variables in the microclimatic analysis are considered relative humidity (RH), interior temperature (T_{in}), outdoor temperature (T_{out}) and variation in the CO_2 concentration. The temperature of the cave interior is mainly affected by the presence of visitors, which may be considered one main cause of thermal disturbance compared to natural variations (Calaforra et al. 2003). Additionally, CO_2 concentration and RH are also affected by human presence.

2.3.1. Discrete Wavelet Transform

By filtering the signals recorded in Rull cave, high-frequency events can be distinguished from low-frequency events and high and low components of the signal can be studied separately. The DWT is implemented as the selected filtering method for the first part of the analysis, as it allows a compact representation of the data with a useful reduction in signal noise. The mother wavelet filter used in DWT analysis is Daubechies 10, which experimentally has been considered appropriate for the study of the analysed microclimatic signals.

Previous works employed discrete wavelet transform (DWT) to filter data series. DWT follows a sub-band coding scheme (Mallat 1989) based on two quadrature filters that work as high-pass (wavelet filter, derived from the respective mother wavelet) and low-pass filters (scaling filter) plus downsampling by a factor of 2. The application of these filters provides two new signals, i.e. the wavelet (or detail) and scaled (or approximation) coefficients. These filters are successively applied on the scaled coefficients for each scale or level of the wavelet decomposition. Thus, for a wavelet decomposition of *L* scales, the approximation signal at scale *L* and the detail signals at scales from *L* to 1, e.g. *L*+1 coefficients, are obtained, each one associated with a theoretical period band. The selected scale to perform the analysis is scale 8. Attending to the sampling frequency, raw signals contain theoretical periodicities ranging from 1.33 to infinite days. Following the decomposition pattern for the DWT, periodicities from 170 to infinite days (which contain 1-year periodicity) are highlighted when selecting scale 8. DWT is performed with the Environmental Wavelet Tool (EWT) (Galiana-Merino et al. 2014). EWT is a MATLAB-based computer code developed for the simultaneous wavelet analysis and filtering of several environmental time series, particularly focused on the analyses of cave monitoring data. The application of the wavelet and scaling filters on finite-length

signals suffers from edge effects that appear in the borders and the gaps of the data series and limit the maximum scale of analysis.

In the literature, numerous approaches and applications of DWT can be found: the analysis of trends in streamflow and precipitation (Nalley et al. 2012; Partal and Kucuk 2006), the assessment of long-term trends in geomagnetic activity (De Artigas et al. 2006), the detection and location of seismic events (Botella et al. 2003; d'Auria et al. 2010; Galiana-Merino et al. 2007, 2008; Hafez et al. 2010), and the analysis of geophysical data series (Percival 2008).

2.3.2. Continuous Wavelet Transform

In this study, CWT is applied on the separated components of the signals (low and high frequency) using the Morlet wavelet. The results obtained when performed CWT analysis will be used afterwards to perform XWT and WTC. In the continuous wavelet transform (CWT), the wavelet function works (although not strictly necessary) as a band-pass filter well located in frequency through a scale parameter and well located in time through a translation parameter and the effective time support of the wavelet used. For the most commonly used wavelet families, the scale is directly proportional to the central period of the wavelet and can be set up to a real number. Thus, the CWT results correspond to the analysis (or filtering) of the signal at some specific period or set of periods (scales). The filtering of any finite-length signal through the wavelet functions produce some edge effects, which reduce the reliability region of the wavelet results.

CWT has been applied in multiple research applications, such as the analysis of soil spatial variations (Biswas and Si 2011) and soil hydraulic properties (Si 2003), filtering of multichannel seismic data (Galiana-Merino et al. 2013), characterization of surface waves (Holschneider et al. 2005; Kulesh et al. 2005 and 2008), the study of wave polarization properties (Diallo et al. 2006; Kulesh et al. 2008) and airborne CO_2 measurements over heterogeneous landscapes (Vadrevu and Choi 2011), the evaluation of meteorological data characteristics (Wang and Lu 2010), and studies focusing on the impact of boundary layer dynamics of atmospheric CO_2 concentration variability (Lac et al. 2013, Pal 2014).

2.3.3. Mother wavelets

Both the choice of an appropriate mother wavelet filter and the wavelet transform depend on the specific application, although the selection is not unique and several choices can provide similar results. With respect to the mother wavelet, they are grouped into different types of wavelet families with different properties. In this work, both Daubechies and Morlet wavelets are used. The Daubechies family offers a compromise between smoothness and compactness (Dohan and Whitfield 1997). Its soft signal variations and shape allow for an easy fit to our type of data. Daubechies wavelets have been employed to analyse seismic signals (e.g., Galiana-Merino et al. 2003, 2004), drilling-ability data (Frantziskonis and Denis 2003)

and precipitation series (Luan et al. 2011). Morlet wavelets are used to find temporal periodicities. Morlet mother wavelets provide a good balance between time and frequency space (Grinsted et al. 2004).

2.3.4. Cross wavelet transform and wavelet coherence

After the identification and extraction of some interesting parts or components of the registered signal through wavelet analysis, the next step is to identify relationships between the obtained new signals along time or frequency to determine common behaviours between them. To achieve this aim, cross wavelet transform (XWT) and wavelet transform coherence (WTC) are calculated between two CWTs.

The study of interrelations between pairs of time-domain signals can be performed by the application of the XWT. A significance test is conducted at every point in the time/scale plane to check the wavelet power. WTC analyses the coherence and phase lag between two time series as a function of both time and frequency. Areas with high common power between signals are identified in XWT and WTC between pairs of signals. In our study, XWT and WTC are implemented with the software provided by Grinsted et al. (2004), which is available as a MATLAB software package.

2.3.5. Resemblance analysis

In this study, resemblance analysis in DWT is performed to identify common behaviours in time series. Coherence function characterises the degree of similarity between signals in the frequency domain. The mean value of the coherence function can be used as an indicator of the similarity between two time series. A high mean value of coherence is obtained when both analysed sequences present a similar frequency composition (Philippidis and Aggelis 2003).

3. Results and discussion

3.1. Rull cave microclimate conditions

The microclimate of Rull cave was continuously controlled for a completed annual cycle (May 2013 - September 2014). Inside the cave, a stable microclimate governs the whole cycle (Fig. 1(a)). The average annual indoor temperature is 15.9°C. The temperature follows an annual cycle, with the highest temperature (16.3°C) occurring during winter and the lowest temperature (15.6°C) occurring in summer. The cavity is well characterised by a high thermal stability, but remarkable (±0.1°C) daily temperature fluctuations inside the cave are detected from March to August, which might be directly related to the highest presence of visitors in this period. These daily fluctuations tend to disappear from September to February. Temperature differences between indoor and outdoor atmospheres vary in describing the same annual pattern of CO_2 and ^{222}Rn concentrations (Fig. 1(b)). Relative humidity (Fig. 1(c)) always remains near saturation (>97%), but an annual pattern is identified for the whole year. Maximum values of relative

humidity (98.9%) occur from September to February, in accordance with temperature. From March to August, the RH values decrease and daily fluctuations (±1%) are noticeable, similar to those that occurred with T_{in}.

Density differences between the cave and the outside air are primarily responsible for the gaseous recharge (April – October) or outgassing state of the cavity (November – March). The gaseous recharge of the cavity occurs when the outdoor temperature is higher than the cave air temperature as a consequence of the air density differences. During this period the cave experiences an isolation state: the gaseous interchange between the underground and exterior atmosphere is limited. On the contrary, the outgassing state of the cavity occurs when the outdoor temperature is lower than the temperature inside the cavity.

In Rull cave, the CO_2 concentration also reveals an annual periodicity (Fig. 1(d)). The amplitude of the CO_2 measurements vary from 565 ppm (February) to 4,065 ppm (September) with an average annual value of 2,216 ppm. The minimum CO_2 concentration of cave air is achieved during the coldest months, whereas in the warmest months, a considerable increase in CO_2 content is registered inside the cavity. ^{222}Rn shows a similar pattern, revealing a strong relationship between both gases. In Rull cave, the ^{222}Rn annual pattern reveals maximum values during summer (nearly 3,500 Bq m^{-3}) and minimum values (513 Bq m^{-3}) in winter, with an annual average concentration of 1,762 Bq m^{-3}. Figure 1(d) shows some problems with ^{222}Rn measurements deduced by the important amount of gaps in the register. The lack of continuity in the ^{222}Rn register is responsible for not performing wavelet analysis with this signal.

Within the cave, the barometric pressure has an average value of 961 mbar, with an oscillation range no greater than 32 mbar (Fig. 1(a)). The barometric pressure inside the cave is completely closed to the environmental barometric pressure at the exterior (average value of 962 mbar), indicating a connection between the external and cave atmospheres.

The mean outside temperature is 17.4°C with notable oscillations throughout the year. In the coldest months, temperatures may reach nearly 0°C, and in the warmest periods, they can exceed 30°C. The relative humidity in the exterior varies from 10 to 70% with an average of 62%. Precipitation is limited in the area. The annual rainfall (September 2013-August 2014) was 276 mm, principally distributed in small events in the fall and spring seasons. Density differences (Fig. 1(b)) were calculated using the ideal gas equation and assuming that the air is a mixture of water vapour and dry-air (Cuezva 2008). For cave air, the CO_2 concentration was taken into account due to the high concentrations of gas, which could affect the absolute value of the air density.

As a consequence of the presence of visitors in Rull cave, the raw recorded signals are composed of low (related to the natural trends of the signal) and high frequencies (influenced by daily cycles, presence of visitors and even by some sporadic meteorological events, such as rainfall). In the following sections, this time-frequency behaviour of CO_2 and the internal and external climatic parameters are described in detail.

3.2. Low-frequency component: Seasonal characteristics

The low-frequency component of CO_2, RH and T_{in} describe a cyclic behaviour (Figs. 2(a) to 2(c)). Both components (low and high frequency) are differentiated from the original recorded signals. Thus, the low-frequency components are released of high-frequency events, which is almost equivalent to affirming that the human impact has been removed from the signals. In Fig. 2, the original signals were filtered using DWT (mother wavelet filter Daubechies 10, scale 8), and their components were differentiated.

The value of coherence between RH and T_{in} is 0.996, which confirms the existing interrelation between them. T_{in} directly depends on the external temperature (T_{out}), although the response of T_{in} is delayed in relation to T_{out}. The maximum T_{in} occurs in January, whereas the maximum T_{out} occurs in August, which indicates a 6-month lag. The main factor responsible for this delay is the low thermal conductivity of the host rock. The rock requires long periods of exposure to outdoor conditions to transmit changes in the indoor conditions (Hoyos et al. 1998). In addition, the ventilation stage, which occurs from November to March, might also contribute to this delay. The highest RH occurs from September to February due to the decrease in T_{in}.

The low-frequency component of the CO_2 signal reveals the two distinguishable states of the cavity in the annual cycle. The CO_2 concentration displays 1-year cycles as a result of the isolation or outgassing state of the cavity. The seasonality of the outside–inside temperatures directly exerts an effect on CO_2 behaviour (Fig. 1). Seasonal temperature variability implies air density differences between the cave and outside air, which control the seasonal ventilation of Rull cave. Throughout the entire cycle, the CO_2 concentration was dependent on the temperature ratio. In the winter, from November to March, ventilation was predominantly driven by air density differences between the cave and the external atmosphere, and air renewal processes maintained CO_2 levels below the average annual concentration. In contrast, from April to October, temperatures inside the cave remained below the external temperature; the cave functioned as a trap for cold and CO_2-enriched air. In 2013, from October 28 to December 1, the CO_2 concentration decreased from 3,569 to 932 ppm, suggesting that a renewal process of the cave air occurred continuously for the entire month.

3.3. High-frequency component

In Fig. 2, the high-frequency components of the signal confirmed the influence of visitors in the cavity microclimate. Signal disturbance is directly related to human presence: major oscillations in the high-frequency components of T_{in} and RH occurred when the number of visitors was higher (April to September-October) and when the cave remained isolated. In addition, CO_2 oscillations detected in the high-frequency component of the signal allowed for detection of major events of visitors.

In Fig. 3, the signals are analysed in pairs: T_{out} and T_{in}, CO_2 and T_{out}-T_{in} differences and CO_2 and rainfall. Relationships between CO_2 and T_{out}-T_{in} differences are evaluated because air density differences (as a consequence of temperature differences) are essential in cave ventilation. To perform the analysis for the whole studied period (May 2013-August 2014), T_{out}-T_{in} differences are used instead of D_{in}-D_{out} differences due to the lack of data of D_{in}-D_{out} differences for the first few months of the studied period.

3.3.1. Temperature differences (T_{out} -T_{in})

In Figs. 3(a) to 3(b), the periodicity at the 1-day band is identifiable when performing XWT and WTC of the high-frequency components. The XWT of T_{out} and T_{in} signals shows regions with large common spectral power in the time-frequency domain. In the 1-day band, signals are phase-related. The WTC graph shows areas of strong correlation between both signals with values close to 1. For all of the scalograms in Fig. 3, the Cone of Influence (curved lines) determines an area where the edge effects cannot be ignored. The border distortion is usually caused by insufficient data points both at the beginning and at the end of finite-duration signals. The edge effect increases with scale and reduces the effective length of the analysed data series.

A total of 20,129 people visited the cavity in the studied period, but in the warmer months (from April to October), the number of visits was 16,860. Thus, nearly 84% of visits occurred in these months. The average weekly value of visitors from April to October is 355, whereas it is 166 from November to March.

The 1-day periodicities are identifiable in months when the cave remains in an isolation state (April to October), coincident with the existing oscillations in RH and T_{in} signals (Figs. 2(a) to 2(b)). On the contrary, when the cave is in an outgassing state, the 1-day periodicities in the T_{out} -T_{in} relationships disappear. Two main causes might be responsible for this. (i) A major T_{out} influence inside the cavity during the isolation state, which is characterized by the daily permanent cycles (day-night). When the cavity is isolated, it is governed by an indoor calm state where the influence of T_{out}, the presence of visitors and any type of disturbance is much more noticeable. In contrast, during the outgassing state, ventilation and air renewal processes buffer the effects of the possible disturbances. (ii) The presence of visitors inside the cavity is accentuated in this period (Fig. 2(d)). A higher visitor regimen provokes an increase in the opening-closing mechanism of the door. This is directly related to the indoor microclimate disturbance and accentuates the 1-day periodicities in RH and T_{in}. In addition, the phase arrows (T_{out} -T_{in}) indicate a change in the behaviour of the signals. They are in phase (pointing right) (Figs. 3(a) to 3(b)) for the whole 1 day-band periodicity (isolation state of the cavity), but there is a short period (November 2013) when the arrows display different characteristics, which might be related to the rapid gaseous discharge of the cavity.

3.3.2. Influence of high-frequency events on the CO_2 signal

From April to October, the low-frequency component of CO_2 reflects the recharge state of the cavity (input efflux of soil produced CO_2 in the cavity), whereas during the winter, an opposite pattern (CO_2-outgassing state) is described by this low-frequency component (Fig. 2(c)). The high-frequency component of CO_2 is evaluated in both states because some differences are noted in the recorded signal. In Figs. 3(c) to 3(d), the 1-day periodicity band is also existent when the CO_2 signal is compared with the T_{out}-T_{in} difference, although the CO_2 signal does not show evident daily cycles by itself compared to those in the T_{in} and RH signals. As cited previously, it seems that the air renewal process when the cave is in a ventilation state buffers the 1-day periodicities.

The high-frequency CO_2 component disturbance in the cavity is caused by different factors: (i) In some cases, rainfall acts as a high-frequency event, causing some disturbance in the CO_2 concentration. The WTC graph between the high-frequency component of CO_2 and rainfall (Figs. 3(e) to 3(f)) shows areas of strong correlation between both signals coincident with precipitation events in August-September 2013, November-December 2013 and March-April 2014. Each rainfall episode produces a quasi-simultaneous increase in the CO_2 concentration inside the cavity (Fig. 1). In particular, the rainfall episode in December 2013 caused a simultaneous increase in CO_2 and ^{222}Rn concentrations. After the rainfall event, dripping points become activated and CO_2-desgassing from drip-water increased. However, CO_2 is mostly transported in the gaseous phase involved in downward dysphasic flow rather than as a dissolved species degassing from supersaturated cave waters (Bourges et al. 2014). The seepage moves through the connected porous system of rock fractures and fissures, and the air trapped in the porous system (CO_2 and ^{222}Rn enriched) is pushed into the cavity. (ii) The most important disturbance in the CO_2 high-frequency component is the result of human impact after a massive visit (i.e., more than 50 people, large groups of scholars or retirees) in the cavity, when the CO_2 concentration increases temporally due to the anthropogenic input of CO_2. For instance, the peak in CO_2 concentration found at the end of September 2013 was caused by a 250-person visit (Figs. 1 and 2). The baseline concentration is recovered after the visit events over a period of time that might depend on the cavity state.

In addition to periodicity at the 1-day band, Fig. 3(c) shows areas of strong correlation between both signals in the 4- to 16-day band during most of the evaluated period. Nevertheless, this is not confirmed with WTC for the same signals. This fact should be carefully interpreted because resonance effects may exist, falsely indicating an important contribution of the two signals at the same frequency band (Veleda et al. 2012). Figure 4 plots the spectral density graph of the visitor regimen for the whole period to evaluate the possible reasons of the 4-16 day band in Fig. 3(c). It is highlighted that predominant frequencies are 0.13 and 0.28 (equivalent to periodicities of 7.7 and 3.6 days), which would be placed in the 4- to 16-day band. These periodicities (7.7 and 3.6 days) are responsible (among other unknown causes) for the 4- to

16-day band. The number of people who visit the cave rises normally at the weekend, but frequently, at midweek, a massive visit (50 people approximately) occurs. This frequency in the weekly visits results in the 4-day periodicity. The influence of visitors on the CO_2 concentration and T_{in} is therefore confirmed. However, to demonstrate the 4- to 16-day scale in a robust manner, a longer time series (i.e., more than 2 years) will be necessary in the future, when there are enough recorded data.

The remarkable relationships between both signals of CO_2 and T_{out}-T_{in} differences were reinforced in November 2013 and April 2014, with periodicities of 4-8 days strongly marked in Fig. 3(c). These two marked areas are coincident with the change of tendency in cave ventilation (Garcia-Anton et al. 2014). In November 2013, the Rull cave changed from an isolation to degasification state, whereas in April 2014, the opposite occurred (Fig. 1(d)). Signal periodicities (CO_2 and T_{out}-T_{in} differences) vary during these events due to the variation of the cavity state.

3.4. Time evolution of the human-induced changes of the cave environmental conditions

Different events have been analysed in detail. They occur both during the isolation and outgassing states of the cavity.

Within the isolation state of the cavity, RH and T_{in} oscillations finished on August 28, 2013 (Fig. 5). Temperature oscillations occurred mainly from May to the middle of August when the low-frequency component of T_{in} remained at the lowest annual values (Fig. 2(b)). Once the low-frequency component of T_{in} showed higher values inside the cavity (middle August), visitors do not have a pronounced impact. This temperature recovery directly affects RH, causing the daily oscillations to be less drastic during the last two weeks of August, and later becoming nearly unidentifiable the first week of September, when the number of visitors accessing the cavity begins to decrease. The 1-day periodicities in the high-frequency component of T_{out} -T_{in} become significant again at the beginning of March 2014, when the low-frequency T_{in} component decreases, and the number of visitors rises simultaneously. This highlights the direct relationship found between the presence of visitors in the cavity and the daily variations in T_{in} and RH influenced as well by the state (isolation or outgassing) of the cavity.

In addition, several days, from April 17th to April 21st (coincident with the Easter Holidays), were analysed. In this period, 1,247 people visited the cave. The high-frequency component of the CO_2 signal (Fig. 6) revealed that 5 days of continuous massive visits (on April 20, 453 visitors entered the cave) resulted in a net increase in the CO_2 concentration of 275 ppm (April 17, 5:30 pm to April 21, 5:30 ppm), whereas the low-frequency component established a natural recharge of 670 ppm for the same period (Fig. 2(c)). As a consequence, due to the huge amount of consecutive visitors in the cave, the CO_2 concentration previous to the massive event was not recovered, and the increase in the CO_2 concentration suffered a cumulative effect. From April 22, the number of visitors gradually decreased, supported by a substantial decrease in

the CO_2 concentration. Each day from April 22 to April 25, the number of visitors was 30, 139, 22 and 38, producing increases of 20, 140, 100 and 140 ppm, respectively. Although 24 h after the visit the concentration values were reduced, the daily increases were not completely recovered from the previous day. A visit of 139 people on April 23 produced a CO_2 increase of 140 ppm that could not be recovered. Two days after consecutive groups of people (22 and 38 visitors), a cumulative effect was responsible for an increase of 140 ppm (April 25). The reduction in the visitor regimen from April 24 to 26 caused the high-frequency component of the signal to suffer a sharp decrease of nearly 500 ppm in less than 24 h. The high-frequency concentration steeply fell, reaching low-frequency levels. In addition, the absence of visitors from April 26 to 28 (by coincidence, no visitors entered the cave during this period) caused the high-frequency concentration to reach low-frequency levels, which are described in this period as an upward tendency.

From April 17 to April 21, T_{in} and RH again displayed daily oscillations (Fig. 6). The presence of daily visitors affected both parameters. For T_{in}, a daily average increase of nearly 0.12°C was coincident with massive visits. A daily cycle is noted in the temperature data, increasing with the first group of visitors around 10:00 am, reaching a maximum temperature at 15:00 pm, and a minimum temperature after midnight. During this period, T_{in} does not recover to the previous values before the visits, showing a cumulative increase of 0.047°C. From April 22, the reduction of visitors allowed for a complete recovery to daily values in T_{in}.

Relative humidity describes a similar behaviour in this event. Daily cycles are correlated to those described by T_{in}. RH increases to a maximum value of 1.5% per day, but the high-frequency component recovers to the previous baseline after the visits events that supposes a no cumulative effect in RH.

In June 2014, when the cavity was still in the same isolation state, a less dense distribution of visitors occurred. From June 23 to 30, an average of 25 people visited the cave daily. Figure 7 reveals that the CO_2 concentration decreased approximately 100 ppm in four days, but no daily variations are detected. The low-frequency component of the signal (Fig. 2(c)) follows an upward trend, whereas the high-frequency component shows an opposite slope. This confirms that natural dynamics are predominant, even with the presence of visitors. Oscillations in T_{in} and RH are noticeable with maximum increases of 0.1°C and 1.05%, respectively. The recovering time of these factors is no longer than 12 hours after the first visit. No cumulative effect is detected.

Within the outgassing state of the cavity, several days in December 2013 were analysed. In the last week of December 2013 (Fig. 8), two consecutive days with more than 50 people produced an increase of nearly 100 ppm in the CO_2 concentration, whereas the low-frequency component decreased (Fig. 2(c)). However, the RH and T_{in} signals were not substantially affected.

From January 17 to January 28, the cave remained completely closed to visitors, although there was an exceptional visit of 55 people on January 22 (Fig. 9). The high- and low-frequency components of the CO_2, T_{in} and RH signals seem to be parallel in a downward trend (Fig. 2). The high-frequency components remain stable because there is no disturbance inside the cavity. However, this visit of 55 people caused an increase of 0.14°C in temperature, which lasted 1 h 30 min. After this time frame, the temperature became identical to the existing value before the event. RH was not affected, remaining constant. The CO_2 increased by 250 ppm, and began to recover 1 h after the visit. In contrast to temperature, the CO_2 concentration reached its previous value on January 25, 72 hours following the event.

Future work will require avoiding the existence of gaps in the data series. To obtain a full understanding of this analysis, it is necessary to use a longer data series of a longer time period. These factors will be taken into account and the proposed methodology and conclusions derived from the impact of visitors to microclimatic conditions will be extended to different cavities, which are presently under study. Therefore, the results presented here can be compared to these additional cavities. An intense insight of the soil-rock system above the cave, matched together with the conclusions obtained in this study, could lead to a deep understanding of the role of underground cavities as contributors in the global CO_2 cycle.

4. Conclusions

The results obtained in this paper of the dynamics of an underground cavity confirm the existence of a seasonal contribution to open atmosphere CO_2-enriched air from these underground environments. The study of CO_2 dynamics and the microclimatic signals of Rull cave was conducted using wavelet analysis. This tool has been demonstrated to efficiently detect signals variations, which can remain hidden in noise in a simple spectrum.

The proposed methodology for analysing environmental data easily detects the disturbance caused in underground cavities by anthropogenic phenomena. Wavelet analysis enables researchers to filter raw signals of monitored parameters. This filtering method allows for dividing a raw signal into two components; the first component indicates the low-frequency events or natural trends of the signal, and the second component indicates the high-frequency events. In touristic caves, such as Rull cave, high-frequency events are mainly related to visitors, particularly when there are no other substantial natural events. In this way, the anthropogenic input of CO_2 in the cavity is perfectly differentiated from the natural input. Moreover, the effect of visitors in the underground microclimate can be characterized. In Rull cave, variations in the microclimate measures due to human presence in the cavity do not exceed natural variations in most of the evaluated months. However, there are some episodes with massive visits, which

cause exceptional variations in the studied parameters that last for long periods before recovered to pre-visit values.

The seasonal pattern (low-frequency component) of trace gases in Rull cave is related to cave ventilation and gas exchange with outside air, mainly controlled by meteorological factors. The main parameters governing the cave's microclimate are differences between outdoor and indoor air temperatures and densities. This seasonal pattern always governs the cave microclimate, which is sometimes affected by visitor disturbances.

Acknowledgements

This research was funded by the Spanish Ministry of Economy and Competitiveness projects CGL2011-25162 and CGL2013-43324-R, and its programme Torres Quevedo (PTQ 13-06296 and PTQ 12-05601). A pre-doctoral research fellowship (BES-2012-053468) was awarded to C. Pla for the project CGL2011-25162. Funding was also provided by the People Programme (Marie Curie Actions – Intra-European Fellowships, call 2013) of the European Union's Seventh Framework Programme (FP7/2007-2013) under REA grant agreement n°624204. The authors thank cave managers for their collaboration throughout the entire investigation. The authors are also extremely grateful to Dr. Sergio Sanchez-Moral for his helpful comments and suggestions.

References

Benavente J, Vadillo I, Carrasco F, Soler A, Liñan C, Moral F (2010) Air carbon dioxide contents in the vadose zone of a Mediterranean karst. Vadose Zone J 9(1): 126-136. doi:10.2136/vzj2009.0027.

Biswas A and Si BC (2011) Application of Continuous Wavelet Transform in Examining Soil Spatial Variation: A Review. Math Geosci 43: 379–396. doi: 10.1007/s11004-011-9318-9.

Botella F, Rosa-Herranz J, Giner JJ, Molina S, Galiana Merino JJ (2003) A real-time earthquake detector with prefiltering by wavelets. Comput Geosci 29: 911-919. doi:10.1016/S0098-3004(03)00099-2.

Bourges F, Genthon P, Genty D, Lorblanchet M, Mauduit E, D'Hulst D (2014) Conservation of prehistoric caves and stability of their inner climate: Lessons from Chauvet and other French caves. Sci Total Environ 493(0): 79-91. doi:10.1016/j.scitotenv.2014.05.137.

Calaforra JM, Fernandez-Cortes A, Sanchez-Martos F, Gisbert J, Pulido-Bosch A (2003) Environmental control for determining human impact and permanent visitor capacity in a potential show cave before tourist use. Environ Conserv 30(2): 160-167. doi:10.1017/s0376892903000146.

Chinarro D, Villarroel JL, Cuchi JA (2012) Wavelet analysis of Fuenmayor karst spring, San Julian de Banzo, Huesca, Spain. Environ Earth Sci 65(8). doi: 10.1007/s12665-011-1351-y.

Cuezva S (2008) Dinámica microambiental de un medio kárstico somero (cueva de Altamira, Cantabria): microclima, geomocrobiología y mecanismos de interacción cavidad/exterior. Tesis Doctoral. Universidad Complutense de Madrid. Madrid, España.

Cuezva S, Fernandez-Cortes A, Benavente D, Serrano-Ortiz P, Kowalski AS, Sanchez-Moral S (2011) Short-term CO_2(g) exchange between a shallow karstic cavity and the external atmosphere during summer: Role of the surface soil layer. Atmos Environ 45(7): 1418-1427. doi: 10.1016/j.atmosenv.2010.12.023.

Daubechies I (1992) Ten lectures on wavelets. CBMS-NSF Regional Conference Series in Applied Mathematics. SIAM 61: 198-202. doi 10.1137/1.9781611970104.

Denis A and Cremoux F (2002) Using the entropy of curves to segment a time or spatial series. Math Geol 34(8): 899-914. doi 10.1023/A:1021302922108.

d'Auria L, Giudicepietro F, Martini M, Orazi M, Peluso R, Scarpato G (2010) Polarization Analysis in the Discrete Wavelet Domain: An Application to Volcano. B Seismol Soc Am 100(2): 670–683. doi: 10.1785/0120090166.

de Artigas M, Elias A, Fernandez-de-Campra P (2006) Discrete wavelet analysis to assess long-term trends in geomagnetic activity. Phys Chem Earth Parts A/B/C 31(1–3): 77-80. doi: 10.1016/j.pce.2005.03.009.

de Carvalho L, Pla C, Galvañ S, Cuevas-Gonzalez J, Andreu JM, Cañaveras JC, Benavente D (2013) Caracterización Petrográfica y Petrofísica de la Roca Encajante de la Cueva del Rull (Vall d'Ebo, Alicante). Macla 17:39–40.

Diallo MS, Kulesh M, Holschneider M, Scherbaum F, Adler F. Characterization of polarization attributes of seismic waves using continuous wavelet transforms. Geophy 2006; 71: 67–77. Doi: 10.1190/1.2194511.

Docampo S, Trigo M, Recio M, Melgar M, Garcia-Sanchez J, Cabezudo B (2011) Fungal spore content of the atmosphere of the Cave of Nerja (southern Spain): Diversity and origin. Sci Total Environ 409(4): 835-843. doi: 10.1016/j.scitotenv.2010.10.048.

Dohan K and Whitfield PH. Identification and characterization of water quality transients using wavelet analysis. 1. Wavelet analysis methodology (1997) Water Sci Technol 36(5): 325-335. doi: 10.1016/s0273-1223(97)00490-3.

Faimon J, Štelcl J, Sas D. Anthropogenic CO_2-flux into cave atmosphere and its environmental impact: A case study in the Císařská Cave (Moravian Karst, Czech Republic) (2006) Sci Total Environ 369(1–3): 231-245. doi:10.1016/j.scitotenv.2006.04.006.

Fernandez-Cortes A, Sanchez-Moral S, Cuezva S, Benavente D, Abella R (2011a) Characterization of trace gases' fluctuations on a 'low energy' cave (Castañar de Íbor, Spain) using techniques of entropy of curves. Int J Climatol 31(1): 127-143. doi: 10.1002/joc.2057.

Fernandez-Cortes A, Cuezva S, Sanchez-Moral S, Porca E, Jurado V, Martin-Sanchez PM, Saiz-Jimenez C (2011b) Detection of human-induced environmental disturbances in a show cave. Environ Sci Pollut R 18(6): 1037-1045. doi: 10.1007/s11356-011-0513-5.

Fernandez-Cortes A, Cuezva S, Garcia-Anton E, Alvarez-Gallego M, Pla C, Benavente D, Cañaveras JC, Calaforra JM, Mattey DP, Sanchez-Moral S (2015) Changes in the storage and sink of carbon dioxide in subsurface atmospheres controlled by climate-driven processes: the case of the Ojo Guareña karst system. Environ Earth Sci. doi 10.1007/s12665-015-4710-2.

Frantziskonis G and Denis A (2003) Complementary entropy and wavelet analysis of drilling-ability data. Math Geol 35(1): 89-103. doi 10.1023/A:1022369213276.

Frisia S, Fairchild I, Fohlmeister J, Miorandi R, Spoetl C, Borsato A (2011) Carbon mass-balance modelling and carbon isotope exchange processes in dynamic caves. Geochim Cosmochim Ac 75(2): 380-400. doi: 10.1016/j.gca.2010.10.021.

Galiana-Merino JJ, Rosa-Herranz J, Giner J, Molina S, Botella F (2003) De-noising of short-period seismograms by wavelet packet transform. B Seismol Soc Am 93(6):2554-2562. doi: 10.1785/0120010133.

Galiana-Merino JJ, Rosa-Herranz J, Giner JJ, Molina S, Botella F (2004) Regularized Deconvolution of Local Short-Period Seismograms in the Wavelet Packet Domain. B Seismol Soc Am 94(4):1467–1475.

Galiana-Merino JJ, Rosa-Herranz J, Jauregui P, Molina S, Giner JJ (2007) Wavelet transform methods for azimuth estimation in local three-component seismograms. B Seismol Soc Am 97(3): 793-803. doi: 10.1785/0120050225.

Galiana-Merino JJ, Rosa-Herranz J, Parolai S (2008) Seismic P phase picking using a kurtosis-based criterion in the stationary wavelet domain. IEEE T Geosci Remote 46(11):3815-3826. doi: 10.1109/TGRS.2008.2002647.

Galiana-Merino JJ, Parolai S, Rosa-Herranz J (2011) Seismic wave characterization using complex trace analysis in the stationary wavelet packet domain. Soil Dyn Earthq Eng 31(11): 1565-1578. doi: 10.1016/j.soildyn.2011.06.009.

Galiana-Merino JJ, Rosa-Herranz JL, Rosa-Cintas S, Martinez-Espla JJ (2013) SeismicWaveTool: Continuous and discrete wavelet analysis and filtering for multichannel seismic data. Comput Phys Commun 184(1): 162-171. doi: 10.1016/j.cpc.2012.08.008.

Galiana-Merino JJ, Pla C, Fernandez-Cortes A, Cuezva S, Ortiz J, Benavente D (2014) EnvironmentalWaveletTool: Continuous and discrete wavelet analysis and filtering for environmental time series. Comput Phys Commun 185(10): 2758-2770. doi: 10.1016/j.cpc.2014.06.011.

Garcia-Anton E, Cuezva S, Fernandez-Cortes A, Benavente D, Sanchez-Moral S (2014) Main drivers of diffusive and advective processes of CO_2-gas exchange between a shallow vadose zone and the atmosphere. Int J Greenh Gas Con 21(0): 113-129. doi: 10.1016/j.ijggc.2013.12.006.

Gregorič A, Vaupotič J, Šebela S (2014) The role of cave ventilation in governing cave air temperature and radon levels (Postojna Cave, Slovenia). Int J Climatol 34(5): 1488-1500. doi: 10.1002/joc.3778.

Grinsted A, Moore J, Jevrejeva S (2004) Application of the cross wavelet transform and wavelet coherence to geophysical time series. Nonlinear Proc Geoph 11:561–566. doi: 10.1007/s00477-013-0745-7.

Hafez AH, Khan M, Kohda T (2010) Clear P-wave arrival of weak events and automatic onset determination using wavelet filter banks. Digit Signal Process 20(3):715–723. doi: 10.1016/j.dsp.2009.10.002.

Holschneider M, Diallo MS, Kulesh M, Ohrnberger M, Lück E, Scherbaum F (2005) Characterization of dispersive surface waves using continuous wavelet transforms. Geophys J Int 163: 463–478. doi: 10.1111/j.1365-246X.2005.02787.x.

Hoyos M, Cañaveras JC, Sanchez-Moral S, Sanz-Rubio E, Soler V (1998) Microclimatic characterization of a karstic cave: Human impact on microenvironmental parameters of a prehistoric rock art cave (Candamo Cave, northern Spain). Environ Geol 33(4): 231-242. doi: 10.1007/s002540050242.

Kaiser G. A friendly guide to wavelets (1994) Birkhauser, Boston, USA. doi 10.1007/978-0-8176-8111-1.

Kell DB (2012) Large-scale sequestration of atmospheric carbon via plant roots in natural and agricultural ecosystems: why and how. Philos T R Soc B 367(1595): 1589–1597. doi: 10.1098/rstb.2011.0244.

Kowalczk AJ, Froelich PN (2010) Cave air ventilation and CO_2 outgassing by radon-222 modeling: how fast do caves breathe? Earth Planet Sci Lett 289:209–219. doi:10.1016/j.epsl.2009.11.010.

Kulesh M, Holschneider M, Diallo MS, Xie Q, Scherbaum F (2005) Modeling of wave dispersion using continuous wavelet transforms. Pure Appl Geophys 162: 843–855. doi: 10.1007/s00024-004-2644-9.

Kulesh M, Holschneider M, Diallo MS (2008) Geophysical wavelet library: Applications of the continuous wavelet transform to the polarization and dispersion analysis of signals. Comput Geosci 34(12): 1732-1752. doi: 10.1016/j.cageo.2008.03.004.

Lac C, Donnelly RP, Masson V, Pal S, Riette S, Donier S, Queguiner S, Tanguy G, Ammoura L, Xueref-Remy I (2013) CO2 dispersion modelling over Paris region within the CO_2-MEGAPARIS project. Atmos Chem Phys 13: 4941-4961. doi:10.5194/acp-13-4941-2013.

Li L, Xu CY, Zhang ZX, Jain SK (2014) Validation of a new meteorological forcing data in analysis of spatial and temporal variability of precipitation in India. Stoch Env Res and Risk A 28(2): 239-252. doi: 10.1007/s00477-013-0745-7.

Luan OH, Wang H, Xia DZ. Complexity analysis of precipitation in changing environment in Chien River Basin, China (2011) Water Sci Eng 4(2): 133-142. doi: 10.3882/j.issn.1674-2370.2011.02.002.

Mallat S. A theory for multiresolution signal decomposition: The wavelet representation (1989) IEEE T Pattern Anal 11: 674-693. doi: 10.1109/34.192463.

Mattey D, Fairchild I, Atkinson T, Jean-Paul L, Ainsworth M, Durell R (2010) Seasonal microclimate control of calcite fabrics, stable isotopes and trace elements in modern speleothem from St Michaels Cave, Gibraltar. Geol Soc London Spec Publ 336: 323-344. doi:10.1144/SP336.17.

Milne AE and Lark RM (2009) Wavelet Transforms Applied to Irregularly Sampled Soil Data. Math Geosci 41: 661-678. doi: 10.1007/s11004-009-9234-4.

Nalley D, Adamowski J, Khalil B (2012) Using discrete wavelet transforms to analyze trends in streamflow and precipitation in Quebec and Ontario (1954-2008). J Hydrol 475: 204-228. doi: 10.1016/j.jhydrol.2012.09.049.

Pal S and Devara PCS (2012) A wavelet-based spectral analysis of long-term time series of optical properties of aerosols obtained by lidar and radiometer measurements over an urban station in Western India. J Atmos Sol-Terr Phy 84-85: 75-87. doi: 10.1016/j.jastp.2012.05.014.

Pal S, Xueref-Remy I, Ammoura L, Chazette P, Gibert F, Royer P, Dieudonné C, Dupont J.-C., Haeffelin M, Lac C, Lopez M, Morille Y, Ravetta F (2012) Spatio-temporal variability of the atmospheric boundary layer depth over the Paris agglomeration: An assessment of the impact of the urban heat island intensity. Atmos Environ 63: 261-275. doi: 10.1016/j.atmosenv.2012.09.046.

Pal S, Lee TR, Phelps S, De Wekker SF (2014) Impact of atmospheric boundary layer depth variability and wind reversal on the diurnal variability of aerosol concentration at a valley site. Sci Total Environ 496: 424-434. doi: 10.1016/j.scitotenv.2014.07.067.

Pal S (2014) Monitoring Depth of Shallow Atmospheric Boundary Layer to Complement LiDAR Measurements Affected by Partial Overlap. Remote Sens 6(9): 8468-8493. doi:10.3390/rs6098468.

Pal S, Lopez M, Schmidt M, Ramonet M, Gibert F, Xueref-Remy I, Ciais P (2015) Investigation of the atmospheric boundary layer depth variability and its impact on the ^{222}Rn concentration at a rural site in France: Evaluation of a year-long measurement. J Geophys Res-Atmos 120(2). doi: 10.1002/2014JD022322.

Partal T and Kucuk M (2006) Long-term trend analysis using discrete wavelet components of annual precipitations measurements in Marmara region (Turkey). Phys Chem Earth 31(18): 1189-1200. doi: 10.1016/j.pce.2006.04.043.

Percival D (2008) Analysis of Geophysical Time Series Using Discrete Wavelet Transforms: An Overview. In: Donner RV and Barbosa SM (eds) Nonlinear Time Series Analysis in the Geosciences. Springer Berlin Heidelberg, pp 61-79. doi: 10.1007/978-3-540-78938-3_4.

Peyraube N, Lastennet R, Denis A, Malaurent P (2013) Estimation of epikarst air PCO2 using measurements of water δ13CTDIC, cave air PCO_2 and $\delta^{13}CCO_2$. Geochim Cosmochim Ac 118: 1-17. doi 10.1016/j.gca.2013.03.046.

Philippidis TP and Aggelis DG (2003) An acousto-ultrasonic approach for the determination of water-to-cement ratio in concrete. Cement Concrete Res 33(4): 525-538. doi: 10.1016/S0008-8846(02)00999-7.

Pitari G, Coppari E, De Luca N, Di Carlo P (2014) Observations and box model analysis of radon-222 in the atmospheric surface layer at L'Aquila, Italy: March 2009 case study. Environ Earth Sci 71(5): 2353-2359. doi: 10.1007/s12665-013-2635-1.

Pla C, Galiana-Merino JJ, Cuevas-Gonzalez J, Andreu JM, Cañaveras JC, Cuezva S, Fernandez-Cortes A, Garcia-Anton E, Sanchez-Moral S, Benavente D (2015) Definition of Microclimatic Conditions in a Karst Cavity: Rull Cave (Alicante, Spain). In: Andreo B, Carrasco F, Duran JJ, Jimenez P, LaMoreaux J (eds) Hydrogeological and Environmental Investigations in Karst Systems. Springer Berlin Heidelberg, pp 497-503. doi: 10.1007/978-3-642-17435-3_56.

Pu J, Yuan D, Zhao H, Shen L (2014) Hydrochemical and PCO_2 variations of a cave stream in a subtropical karst area, Chongqing, SW China: piston effects, dilution effects, soil CO_2 and buffer effects. Environ Earth Sci 71(9): 4039-4049. doi: 10.1007/s12665-013-2787-z.

Rajaee T (2011) Wavelet and ANN combination model for prediction of daily suspended sediment load in rivers. Sci Total Environ 409(15):2917-2928. doi: 10.1016/j.scitotenv.2010.11.028.

Rivas-Martinez S. Pisos bioclimáticos de España. Lazaroa 1984; 5: 33-43.

Sanchez-Cañete EP, Serrano-Ortiz P, Domingo F, Kowalski AS (2013) Cave ventilation is influenced by variations in the CO_2-dependent virtual temperature. Int J Speleol 42(1): 1-8. doi: 10.5038/1827-806X.42.1.1.

Si BC (2003) Scale and location-dependent soil hydraulic properties in a hummocky landscape: A wavelet approach. In: SelimSelim HM, Pachepsky Y, Radcliffe DE (eds) Scaling Methods in Soil Physics. CRC Press, pp 163-177. doi: 10.1201/9780203011065.ch10.

Serrano-Ortiz P, Roland M, Sanchez-Moral S, Janssens IA, Domingo F, Godderis Y, Kowalski AS (2010) Hidden, abiotic CO_2 flows and gaseous reservoirs in the terrestrial carbon cycle: Review and perspectives. Agr Forest Meteorol 150: 321-329. doi:10.1016/j.agrformet.2010.01.002.

Strang G and Nguyen T (1996) Wavelets and Filter Banks. Wellesley-Cambridge Press.

Vadrevu KP and Choi Y (2011) Wavelet analysis of airborne CO_2 measurements and related meteorological parameters over heterogeneous landscapes. Atmos Res 102(1-2): 77-90. doi:10.1016/j.atmosres.2011.06.008.

Valladares DL, da Silva AAR, Lacerda T, Anjos RM, Rizzotto M, Velasco H, de Rosas JP, Tognelli G, Yoshimura EM, Juri Ayub J (2014) Using ^{222}Rn as a tracer of geodynamical processes in underground environments. Sci Total Environ 468–469:12-18. doi: 10.1016/j.scitotenv.2013.08.003.

Veleda D, Montagne R, Araujo M (2012) Cross-wavelet bias corrected by normalizing scales. J Atmos Ocean Tech 29(9): 1401-1408. doi: 10.1175/JTECH-D-11-00140.1.

Wang N and Lu C (2010) Two-Dimensional Continuous Wavelet Analysis and Its Application to Meteorological Data. J Atmos Ocean Tech 27(4): 652-666. doi: 10.1175/2009JTECHA1338.1.

Wickerhauser MV (1994) Adapted Wavelet Analysis from Theory to Software. CRC Press. doi 10.1137/1038018.

Figures

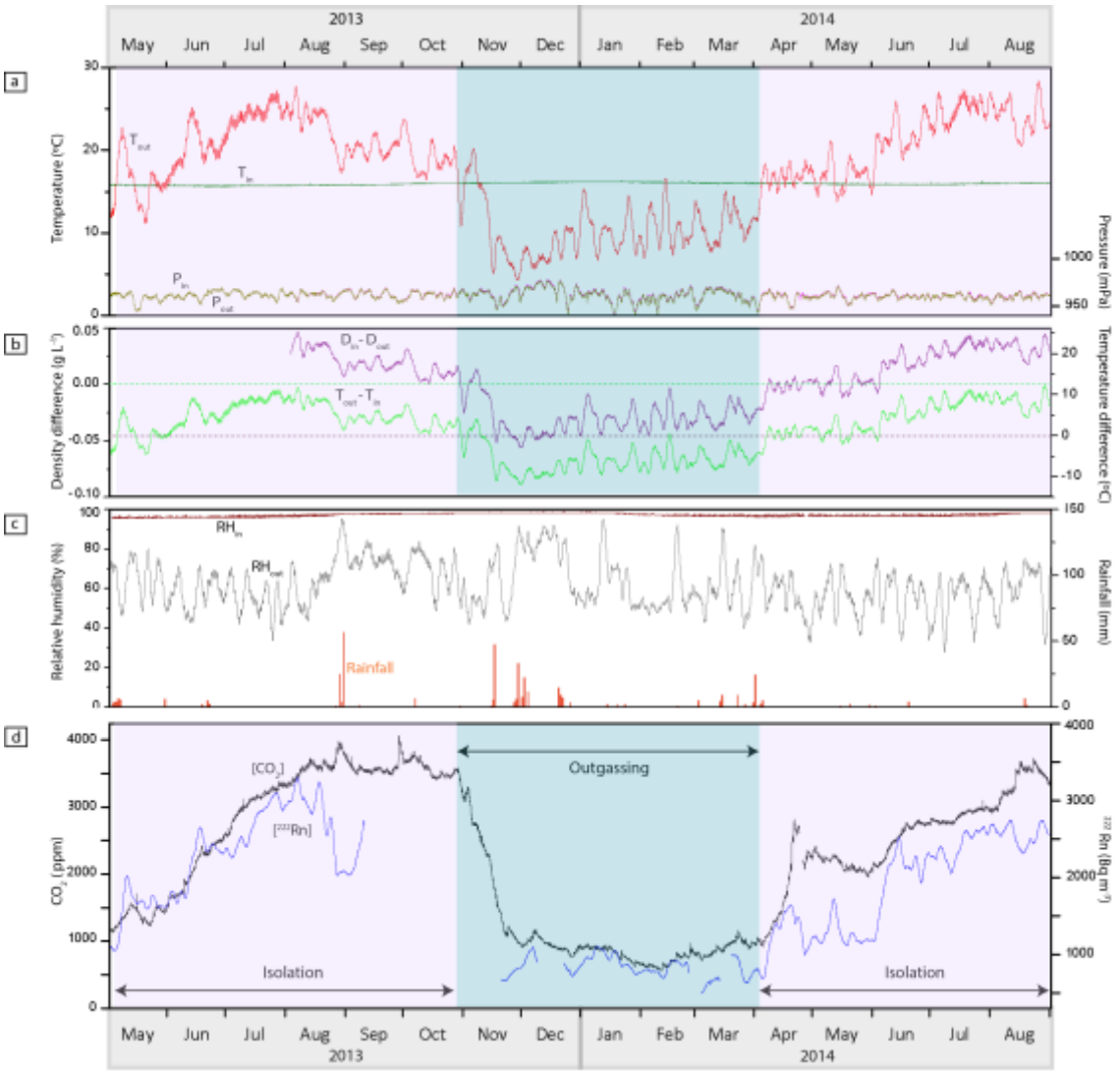

Fig. 1 Time series of the main environmental parameters in Rull cave (May 2013 – September 2014). (a) Indoor and outdoor air temperature and pressure. (b) Air temperature and air density differences. (c) Rainfall, indoor and outdoor relative humidity. (d) $[CO_2]$ and $[^{222}Rn]$.

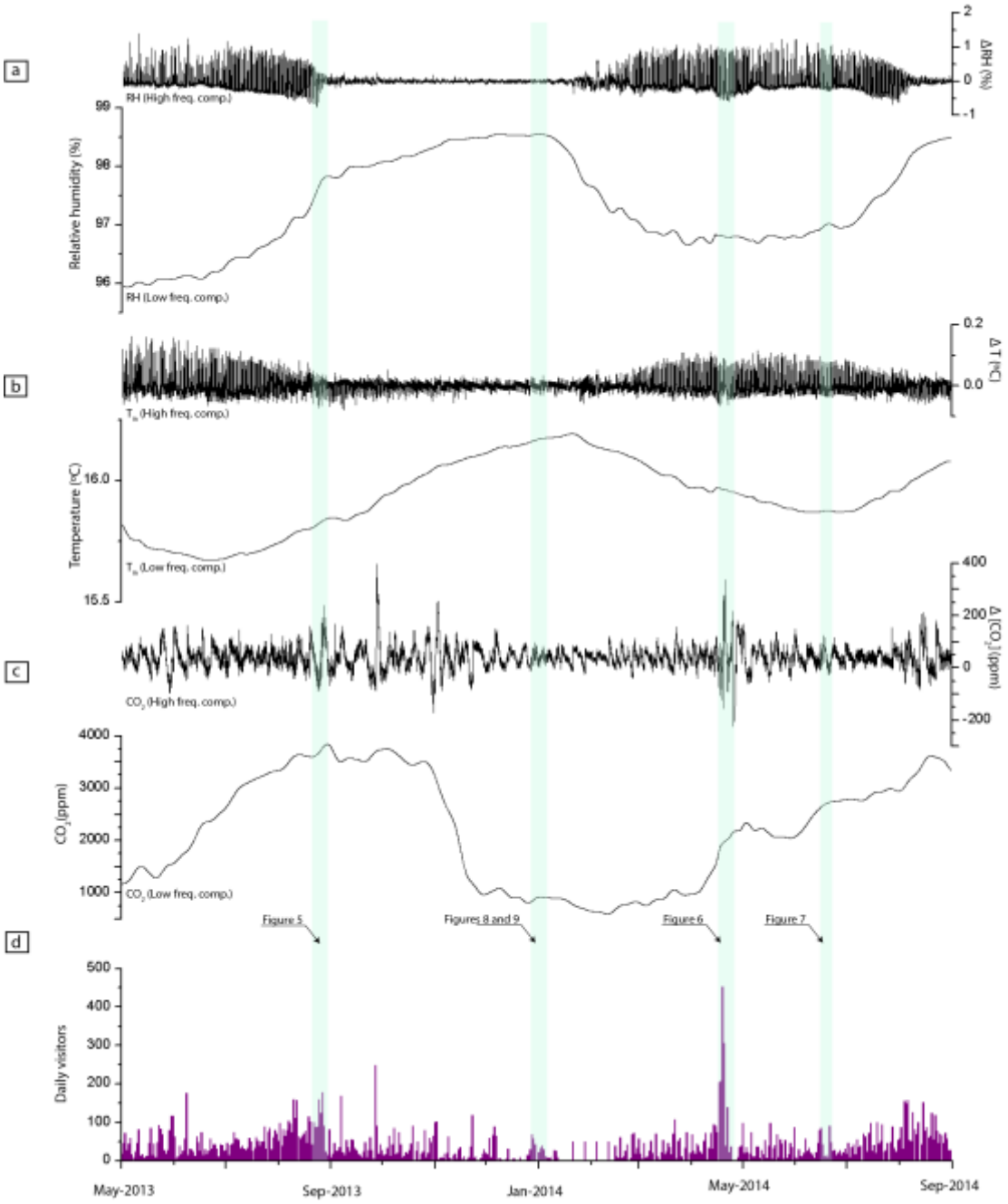

Fig. 2 High and low-frequency components of indoor RH (a), Tin (b) and [CO_2] (c). Signals are obtained by applying DWT using 8 and Daubechies 10 as scale and mother wavelet filter, respectively. (d). Daily visitors inside the cavity.

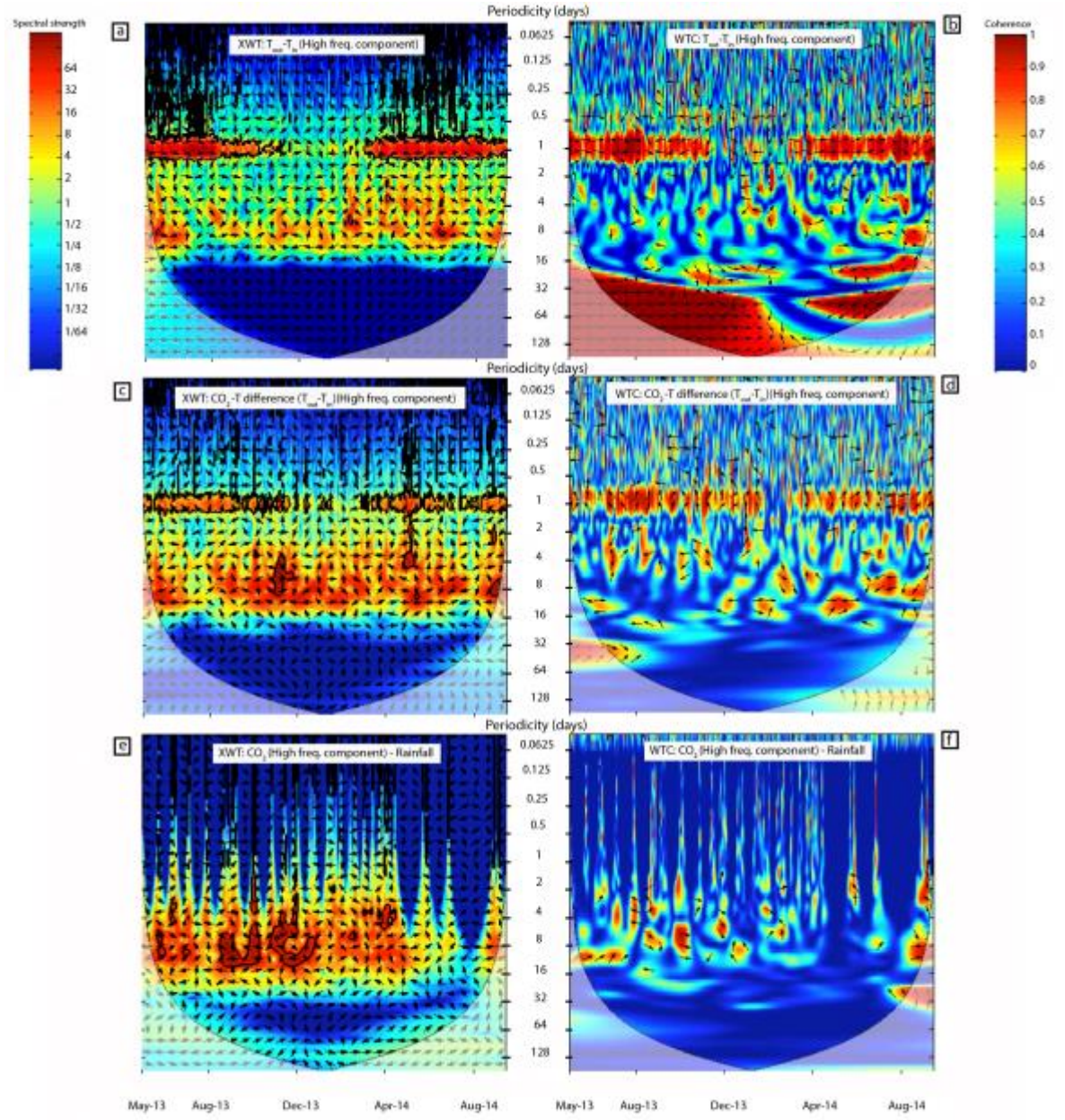

Fig. 3 XWT and WTC between signals: (a,b) T_{out}-T_{in} (c,d) CO_2-(T_{out}-T_{in}) (e,f) CO_2-rainfall. Spectral strength and coherence range from dark (weak) to light (strong) colors. Arrows indicate the relative phase relationship (in-phase pointing right, anti-phase pointing left, one signal leading the other by 900 pointing up/down). Curved lines on scalograms indicate the Cone of Influence where edge effects become important.

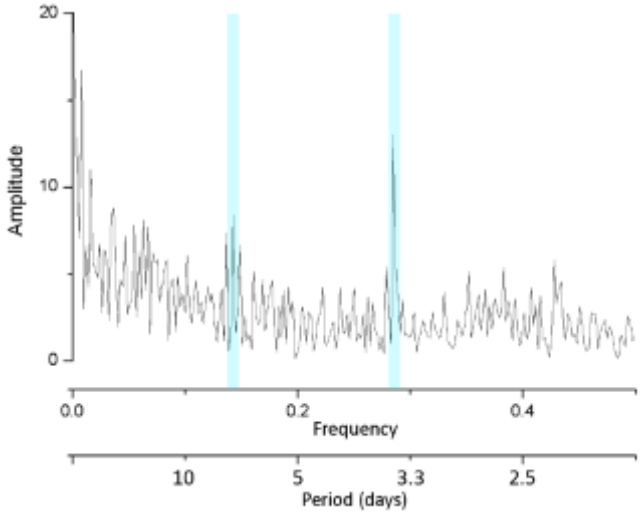

Fig. 4 Spectral density diagram of visitors regimen for the whole studied period.

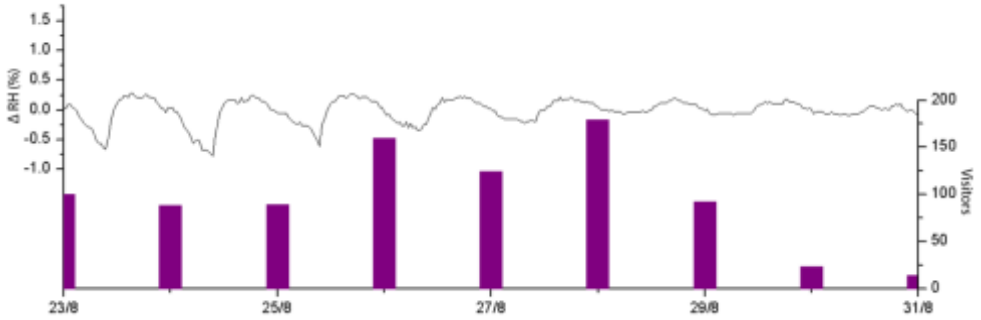

Fig. 5 Detail of RH signal (High-frequency component, August 2013).

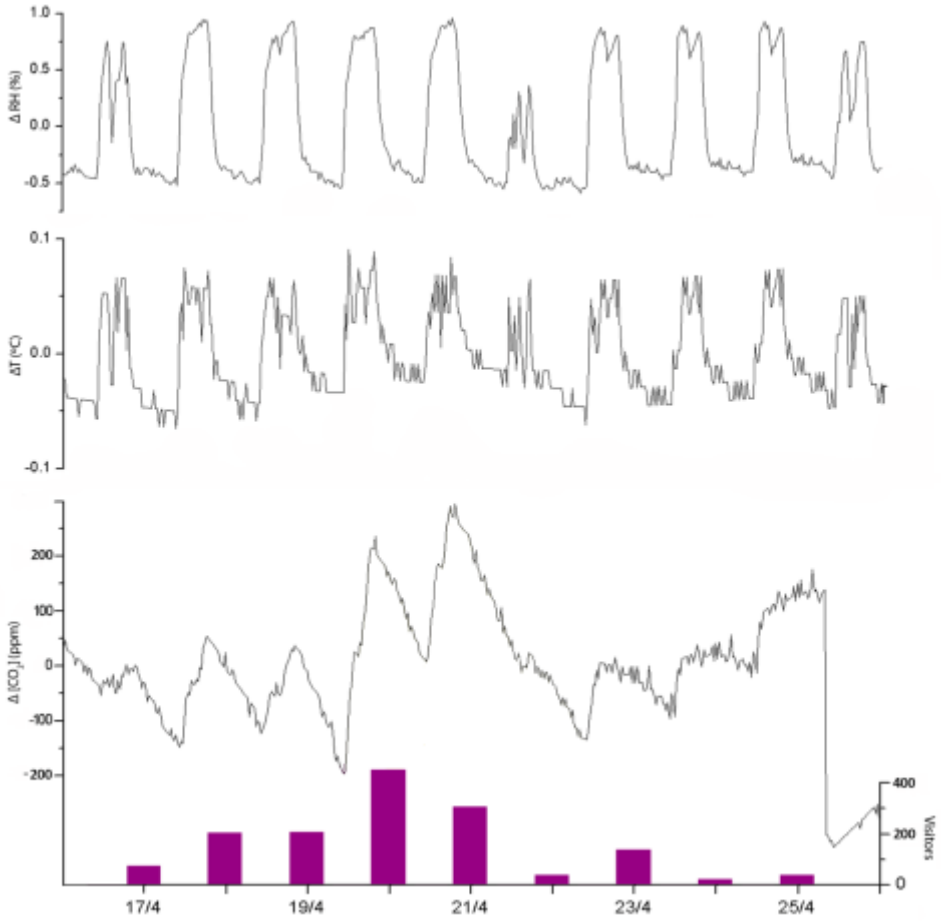

Fig. 6 Detail of RH, T_{in} and CO_2 signals (High-frequency component, April 2014).

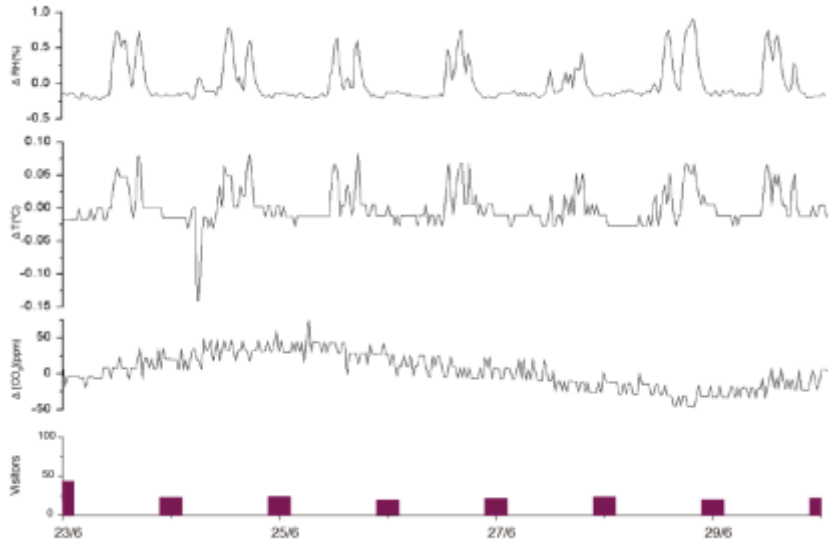

Fig. 7 Detail of RH, T_{in} and CO_2 signals (High-frequency component, June 2014).

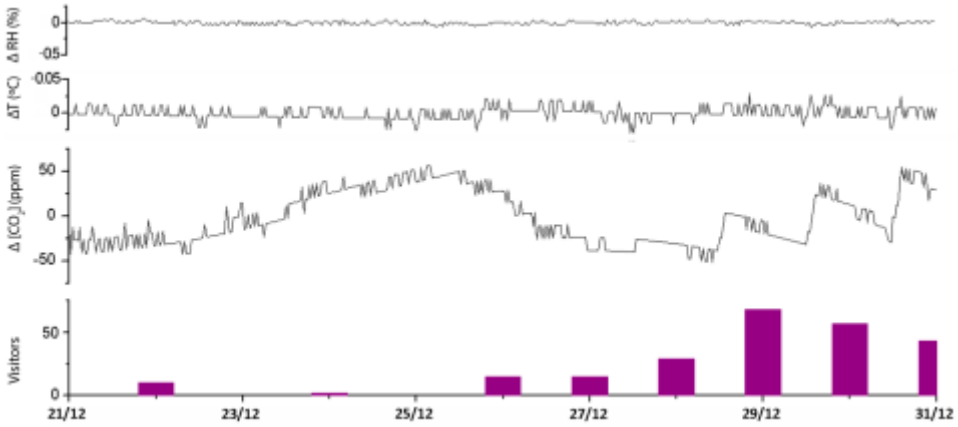

Fig. 8 Detail of RH, T_{in} and CO_2 signals (High-frequency component, December 2013).

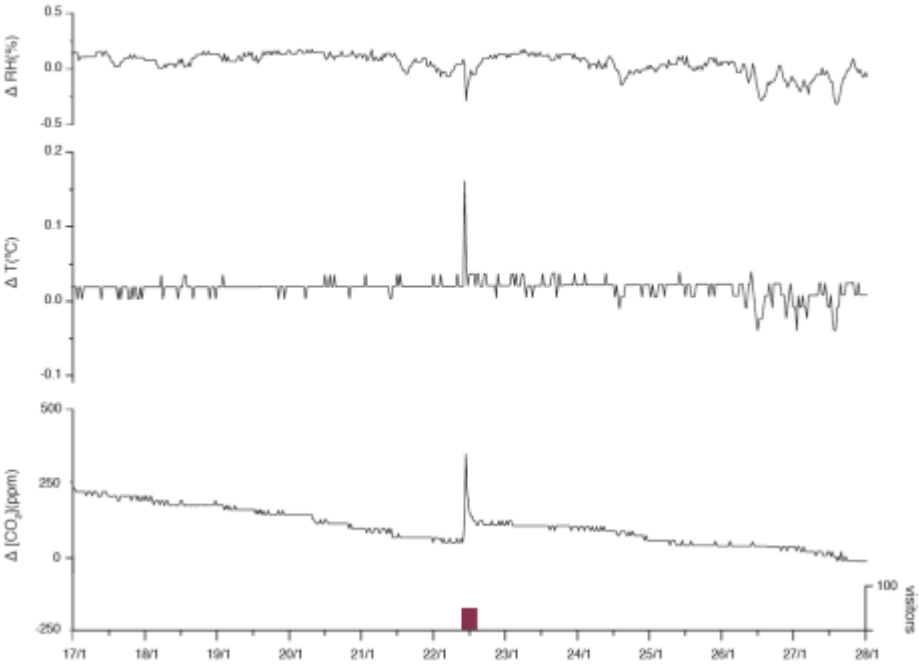

Fig. 9 Detail of RH, T_{in} and CO_2 signals (High-frequency component, January 2014).